RSC Advances

PAPER

View Article Online
View Journal | View Issue

Cite this: *RSC Adv.*, 2024, **14**, 27265

Reaction of methylene blue with OH radicals in the aqueous environment: mechanism, kinetics, products and risk assessment†

Quan V. Vo, *[a] Luu Thi Thu Thao,[b] Tran Duc Manh,[b] Mai Van Bay,[b] Bich-Tram Truong-Le,[c] Nguyen Thi Hoa[a] and Adam Mechler [d]

Methylene Blue (**MB**) is an industrial chemical used in a broad range of applications, and hence its discharge is a concern. Yet, the environmental effects of its degradation by HO˙ radicals have not been fully studied yet. This study employs quantum chemical calculations to investigate the two-step degradation of **MB** by HO˙ radicals in aqueous environments. It was found that **MB** undergoes a rapid reaction with the HO˙ radical, with an overall rate constant of 5.51×10^9 to 2.38×10^{10} M^{-1} s^{-1} and has a rather broad lifetime range of 11.66 hours to 5.76 years in water at 273–383 K. The calculated rate constants are in good agreement with the experimental values ($k_{calculation}/k_{experimental} = 2.62$, pH > 2, 298 K) attesting to the accuracy of the calculation method. The HO˙ + **MB** reaction in water followed the formal hydrogen transfer and radical adduct formation mechanisms, yielding various intermediates and products. Based on standard tests these intermediates and some of the products can pose a threat to aquatic organisms, including fish, daphnia, and green algae, they have poor biodegradability and have the potential to induce developmental toxicity. Hence **MB** in the environment is of moderate concern depending on the ratio of safe to harmful breakdown products.

Received 27th July 2024
Accepted 21st August 2024

DOI: 10.1039/d4ra05437g

rsc.li/rsc-advances

1. Introduction

Methylene blue (**MB**, Fig. 1) is an aromatic heterocyclic dye that is extensively used in industry, especially for coloring silk, cotton, wool, paper, and similar materials.[1–3] **MB** is a cationic dye that is difficult to degrade in natural processes;[4,5] therefore, it has the potential to disrupt ecological systems and in an uncontrolled release to cause a variety of health hazards to humans,[2,3] albeit it also has well-established clinical uses.[6–8] Consistently, the elimination of **MB** from drinking water is a critical concern.[9–14]

Several techniques such as UV-based advanced oxidation processes (AOPs), photocatalytic methods, and ultra-sonic treatments are in use for the decomposition of toxic chemicals including **MB** from waste water.[1,11,15–20] The pulsed power technique can entirely remove **MB** in alkaline solutions within 6–8 minutes.[11] **MB** degradation can be greatly enhanced by using the vacuum-ultraviolet/ultraviolet/persulfate process in comparison to the conventional ultraviolet/persulfate process.[15] The degradation of **MB** in water treatment can also be enhanced by using photocatalysts such as TiO_2 and ZnO; ultrasonic irradiation is also an efficient method.[1,17,20–22] Arguably the simplest approach is supplementing naturally occurring reactive oxygen species (ROS, including HO˙, $SO_4^{\bullet-}$, Cl˙, ClO˙, HOO˙ and $O_2^{\bullet-}$) for the AOPs technique. Of these, HO˙ radicals are known to be the primary active substances for **MB** oxidation.[16,19]

HO˙ radicals are key natural oxidizing species in natural aquifers due to their strong reactivity towards organic substrates,[23,24] playing a substantial role in defining the environmental fate of industrial chemicals despite their low steady-state concentrations ranging from 10^{-18} to 10^{-15} M.[25–27] Therefore, principal photo-oxidation products are expected to form with the involvement of HO˙ in the self-cleaning process of water in nature. Multiple empirical studies have been carried out to determine the rate of the **MB** + ˙OH reaction and to

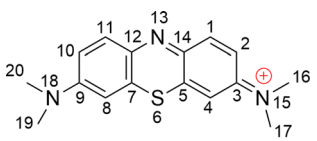

Fig. 1 Structure of **MB**.

[a]*The University of Danang – University of Technology and Education, Danang 550000, Vietnam. E-mail: vvquan@ute.udn.vn*

[b]*The University of Danang – University of Sciences and Education, Danang 550000, Vietnam*

[c]*Department of Science and International Cooperation, The University of Danang, Danang 550000, Vietnam*

[d]*Department of Biochemistry and Chemistry, La Trobe University, Victoria 3086, Australia*

† Electronic supplementary information (ESI) available. See DOI: https://doi.org/10.1039/d4ra05437g

identify the products of **MB** oxidation that occur in an aqueous solution through the introduction of $^{\bullet}OH$.[9,10,15,16,28–30] The rate constant for the interaction of **MB** with $^{\bullet}OH$ at ambient temperature was determined to be 3.8×10^9 M^{-1} s^{-1}.[15] This indicates that **MB** reacts quickly with $HO^{\bullet}$ in water. In spite of the promising results, no further studies have been performed on the kinetics of the process.

The $HO^{\bullet}$ + **MB** reaction proceeds principally through the radical adduct formation (RAF) mechanism of $HO^{\bullet}$ radicals into the aromatic ring. Therefore the predominant intermediates of the $HO^{\bullet}$ + **MB** reaction are the adduct cations detected by mass spectrometry at $m/z = 300$,[28] whereas a two-step reaction of **MB** with $HO^{\bullet}$ radicals yields products at $m/z = 316$.[10,11,28] To explain the mass spectrometry results the addition of $HO^{\bullet}$ radicals into the C1 and C11 positions was proposed.[2,10,11] However, there is no evidence supporting this mechanism. Furthermore, it was noted that the degradation of **MB** occurs slowly in the natural environment and thus the formation of intermediates that may cause toxicity for organic molecules cannot be neglected. Yet the safety of these intermediates has not attracted any attention thus far.

Quantum chemical calculations are well established as a reliable method for determining thermodynamic and kinetic properties of chemical reactions, including radical reactions.[31–35] Here we present a computational study of the thermodynamic and kinetic properties of the hydroxyl radical reactions that involve **MB** and related compounds, as well as the intermediate product reactions that take place within the specified environmental conditions. The toxicity, developmental toxicity, mutagenicity, bioconcentration, and biodegradability of **MB** and its degradation products were also evaluated.

2. Computational methods

Kinetic calculations were performed using the Quantum Mechanics-based Overall Free Radical Scavenging Activity (QM-ORSA) protocol[31] which is directly applicable in this case.[36,37] Eqn (1) was the basis of calculating the rate constant (k) by the application of transition state theory (TST) under standard conditions of 1 M at varying ambient temperatures (253–323 K for the gas phase and 283–323 K for water).[38–44]

$$k = \sigma\kappa \frac{k_B T}{h} e^{-(\Delta G^{\neq})/RT} \quad (1)$$

The reaction symmetry number is denoted by σ.[45,46] Tunneling corrections are represented by κ and were calculated using the Eckart barrier,[47] k_B represents the Boltzmann constant, h is the Planck constant, and $\Delta G^{\neq}$ is the Gibbs free energy of activation. The Marcus theory was used to determine the reaction barriers of single electron transfer (SET) reactions in the solvent.[48,49] Eqn (2) and (3) were used to calculate the $\Delta G^{\neq}$ for the SET reaction.

$$\Delta G_{SET}^{\neq} = \frac{\lambda}{4}\left(1 + \frac{\Delta G_{SET}^{0}}{\lambda}\right)^2 \quad (2)$$

$$\lambda \approx \Delta E_{SET} - \Delta G_{SET}^{0} \quad (3)$$

For SET reaction, the nonadiabatic energy difference between the reactants and the products is represented by ΔE_{SET}, while the conventional Gibbs free energy change of the reaction is denoted by ΔG_{SET}^{0}.[50,51] An adjustment was made for rate constants around the diffusion limit.[47] The steady-state Smoluchowski rate constant (k_D) was estimated from the literature, and the apparent rate constants (k_{app}) for an irreversible bimolecular diffusion-controlled process in solvents[52] were computed using Collins–Kimball theory.[50,53]

$$k_{app} = \frac{k_{TST} k_D}{k_{TST} + k_D} \quad (4)$$

$$k_D = 4\pi R_{AB} D_{AB} N_A \quad (5)$$

$D_{AB} = D_A + D_B$ (denotes the mutual diffusion coefficient of A and B),[52,54] where D_A or D_B is obtained using the Stokes–Einstein formulation (6).[55,56]

$$D_{A\text{ or }B} = \frac{k_B T}{6\pi\eta a_{A\text{ or }B}} \quad (6)$$

η is the viscosity of the solvent (*i.e.* $\eta(H_2O) = 8.91 \times 10^{-4}$ Pa s) and a is the radius of the solute.

Energy minimization was applied to all conformers of species with multiple conformers; the conformer with the lowest electronic energy was used in the study.[57] Each transition stage was characterized by the exclusive existence of a single imaginary frequency. Calculations of intrinsic coordinates were conducted in order to verify the accurate connection between each transition state and the pre- and post-complexes. In addition, the pre- and post-complexes were incorporated into the kinetic calculations.[32,58]

The calculations for this work were conducted using the Gaussian 16 software package[59] at the M06-2X/6-311++G(d,p) level of theory, known for providing precise thermodynamics and kinetics results given the current computational resources.[37,60,61] The SMD methodology was employed to simulate the solvent effects of water,[60] a typical method for assessing the radical scavenging properties of antioxidants. The calculated values showed moderate differences compared to the experimental results, with a k_{calc}/k_{exp} ratio ranging from 0.3 to 2.9.[32,37,43,62–66]

The ecotoxicity assessment was carried out using the Ecological Structure-Activity Relationship Model (ECOSAR V2.0), which has a proven efficacy in assessing the ecotoxicity of organic contaminants.[33,67–70] The developmental toxicity and mutagenicity of **MB** and its transformed products were evaluated through toxicological analysis utilizing the T.E.S.T. (Toxicity Estimation Software Tool) toxicity assessment software.[71] Utilizing the BCFBAF module of EPISUITE, the biological concentration factors (BCFs) produced by the conversion products of **MB** degradation were calculated. Utilizing the BIOWIN 3 & 4 model integrated into the EPISUITE software,[72] an assessment was made of the biodegradability of **MB** and its degradation products.

Table 1 Computed $\Delta G^{\neq}$ (kcal mol^{-1}), κ, k_{app}, $k_{overall}$ (M^{-1} s^{-1}), and Γ (%) at 298.15 K, in the HO$^{\bullet}$ + **MB** in water[a]

Mechanisms	Positions	$\Delta G^{\neq}$	κ	k_{app}	Γ	Intermediates
SET		10.1	0.4[a]	2.50×10^{5}	0.0	**ISET**
FHT	C16–H	5.3	1.0	1.90×10^{9}	18.6	**I16**
	C17–H	5.4	1.0	1.75×10^{9}	17.1	**I17**
RAF	C1	8.2	1.2	1.50×10^{7}	0.1	**I1**
	C2	4.1	1.0	2.07×10^{9}	20.2	**I2**
	C3	8.4	1.2	9.50×10^{6}	0.1	**I3**
	C4	1.8	1.0	2.69×10^{9}	26.3	**I4**
	C5	10.8	1.2	2.00×10^{5}	0.0	**I5**
	C14	4.6	1.0	1.79×10^{9}	17.5	**I14**
	N13	14.7	1.8	1.90×10^{2}	0.0	**I13**
$k_{overall}$				$\mathbf{1.02 \times 10^{10}}$		

[a] The nuclear reorganization energy (λ, in kcal mol^{-1}).

3. Results and discussion

3.1. Reaction of hydroxyl radical with MB in water

3.1.1. The initial reaction of MB with HO$^{\bullet}$ in water. Deprotonation plays a crucial role in the interaction between organic molecules and free radical species in aqueous media.[33,73] Hence, when evaluating the efficacy of water in eliminating radicals, it is essential to consider the deprotonation of **MB**. The pK_a value of **MB** has been previously documented as zero (Fig. S1, ESI†).[74] Thus, in the natural aqueous environment (pH > 2), diphenylamine exists in a cation state (**MB**, Fig. S1, ESI†). Therefore, this state should be used to evaluate the kinetics of the **MB** + HO$^{\bullet}$ reaction in the aqueous environment.

The reaction between **MB** and HO$^{\bullet}$ can occur *via* the radical adduct formation (RAF), formal hydrogen transfer (FHT), or SET, as per eqn (7)–(9):[33,36,37,75]

$$\text{RAF: } \mathbf{MB}\text{–H} + \text{HO}^{\bullet} \rightarrow [\text{HO–}\mathbf{MB}\text{–H}]^{\bullet} \quad (7)$$

$$\text{FHT: } \mathbf{MB}\text{–H} + \text{HO}^{\bullet} \rightarrow \mathbf{MB}^{\bullet} + \text{H}_2\text{O} \quad (8)$$

$$\text{SET: } \mathbf{MB}\text{–H} + \text{HO}^{\bullet} \rightarrow [\mathbf{MB}\text{–H}]^{\bullet+} + \text{HO}^{-} \quad (9)$$

The kinetics of these reactions were calculated and are presented in Table 1, whereas the effect of temperature on the degradation of **MB** is shown in Fig. 2. We found that the reaction between **MB** and HO$^{\bullet}$ radicals had an overall rate constant ($k_{overall}$) of 1.02×10^{10} M^{-1} s^{-1}. This is consistent with the observed experimental rate constant ($k_{exp} = 3.8 \times 10^{9}$ M^{-1} s^{-1}).[15] The FHT reactions at C16/17–H accounted for approximately 35.7% of the total rate constant, while the SET reaction had no contribution ($\Gamma = 0\%$) to the **MB** + HO$^{\bullet}$ reaction. The **MB** + HO$^{\bullet}$ reaction was predominantly taking place *via* the RAF reactions, which represented 64.2% of the reaction. The RAF (C2, C4, and C14) took place rapidly with a rate constant similar to the rate of diffusion ($k \approx 10^{9}$ M^{-1} s^{-1}) and formed the cations [**MB**–OH]$^{+}$ ($m/z = 300$) that were also observed in the experimental studies.[11,28] On the other hand, the RAF reaction at the C1, C3, and C5 sites had moderate reaction rates ($k = 10^{5}$ to 10^{7} M^{-1} s^{-1}) and did not have any impact on the overall reaction. Therefore, the formation of cations [**MB**–OH]$^{+}$ ($m/z = 300$) can occur by introducing HO$^{\bullet}$ radicals to the C2, C4, or C14 sites (Fig. 3), but not at the C1 position, this is also consistent with prior research.[11,28] The likely cause for the preferential adduct formation could be attributed to the presence of the electron-donating group N(CH$_3$)$_2$ in either the *ortho*- or *para*-position. This group has the potential to stabilize both the transition states and the resultant radicals.

The incorporation of HO$^{\bullet}$ radicals into the N13 position is expected to be extremely rare with the highest activation energy ($\Delta G^{\neq} = 14.7$ kcal mol^{-1}) and the lowest rate constant ($k = 1.90 \times 10^{2}$ M^{-1} s^{-1}). Therefore, this reaction does not contribute to the destruction of **MB** by HO$^{\bullet}$ radicals. The primary intermediates of the **MB** + HO$^{\bullet}$ reaction were **I2** (20.2%), **I4** (26.3%), **I14** (17.5%), **I16** (18.6%), and **I17** (17.1%), as indicated in Table 1 and Fig. 3. Therefore, these intermediates were used as

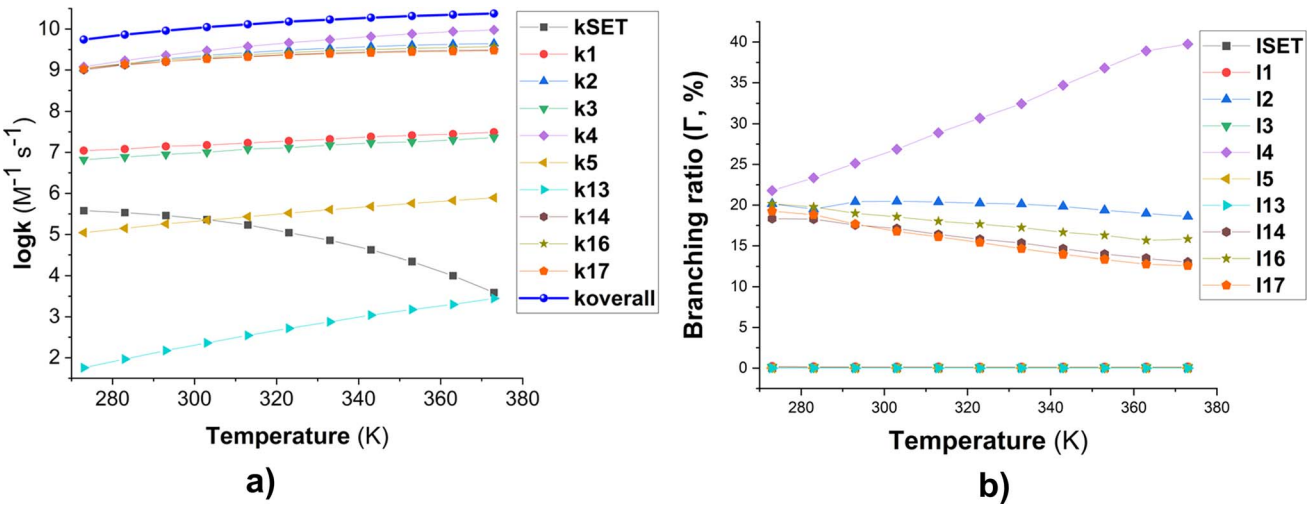

Fig. 2 Temperature dependence of apparent rate constants (log k) in water in the range of 273–373 K ((a) the **MB** + HO$^{\bullet}$ reactions; (b) branching ratio (Γ, %) of the **MB** + HO$^{\bullet}$ reactions; $k_i = 1$–17: the rate constants of the positions in Table 1).

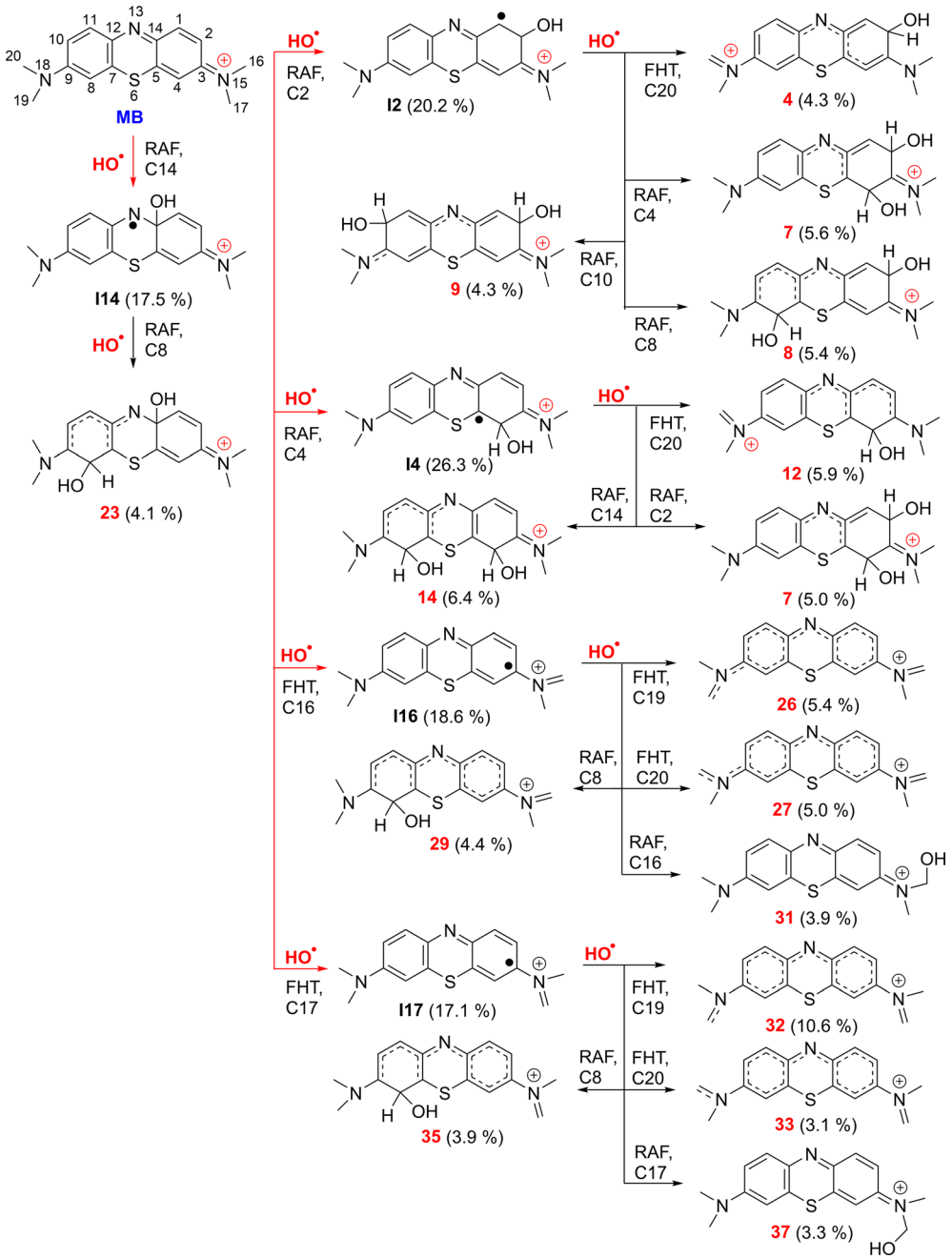

Fig. 3 The selected mechanisms and % products ($\Gamma \geq 3\%$) of the two steps HO$^{\bullet}$ + **MB** reactions in water at 298.15 K.

a starting point for assessing the kinetics of the subsequent reaction step.

To examine the effect of temperature on the degradation of **MB** in water, we determined the rate constants for each reaction in the range of 273 to 383 K (Fig. 2). The rate constants for all reactions increase as the temperature rises with the exception of the SET reaction, where the rate decreased from 3.80×10^5 to 3.90×10^3 M^{-1} s^{-1}. The overall rate constants exhibited a 4.33-fold increase, rising from 5.51×10^9 to 2.38×10^{10} M^{-1} s^{-1} (Fig. 2a). The FHT and RAF (C2, C4, and C14) reactions defined the overall rate constants of the **MB** + HO$^{\bullet}$ reaction at all temperatures investigated. However, the RAF reactions at C1, C3, C5, and N13 did not contribute to the degradation of **MB** by HO$^{\bullet}$ radicals.

As the temperature increases, the major intermediates for the **MB** + HO$^{\bullet}$ reaction, shown in Fig. 2b, exhibit varying branching ratios. Specifically, the percentages of **I2** change from 20.2% to 18.6%, **I4** changes from 21.8% to 39.7%, **I14** goes from 18.3% to 13.0%, **I16** changes from 20.2% to 15.8%, and **I17** from 19.2% to 12.6%. Thus when the temperature climbed, the fraction of intermediate **I4** grew, while the amount of all other intermediates decreased. Percentage-wise **I4** is the main intermediate in all of the studied temperatures.

Table 2 Computed $\Delta G^{\neq}$ (kcal mol^{-1}), κ, k_{app}, k_r, $k_{overall}$ (M^{-1} s^{-1}), and Γ (%) at 298.15 K, in the HO˙ + **MB**-intermediates in water

States	Mechanism		$\Delta G^{\neq}$	κ	k_{app}	k_r	Γ	Products
I2	FHT	C16	8.9	4.4	2.40×10^7	4.86×10^6	0.1	**1**
		C17	9.0	4.6	2.10×10^7	4.25×10^6	0.1	**2**
		C19	6.4	5.1	1.10×10^9	2.23×10^8	2.4	**3**
		C20	5.7	4.9	2.00×10^9	4.05×10^8	4.3	**4**
	RAF	C1	5.8	1.3	3.60×10^8	7.29×10^7	0.8	**5**
		C3	5.6	1.2	4.50×10^8	9.11×10^7	1.0	**6**
		C4	2.5	1.0	2.60×10^9	5.26×10^8	5.6	**7**
		C8	2.7	1.1	2.50×10^9	5.06×10^8	5.4	**8**
		C10	3.7	1.1	2.00×10^9	4.05×10^8	4.3	**9**
		C14	5.0	1.1	9.40×10^8	1.90×10^8	2.0	**10**
	$k_{overall}$ (r) (**I2** + HO˙)					**2.43×10^9**	25.9	
I4		C19	6.5	1.1	3.30×10^8	8.68×10^7	0.9	**11**
		C20	6.2	12.3	2.10×10^9	5.52×10^8	5.9	**12**
	RAF	C1	7.1	1.2	4.50×10^7	1.18×10^7	0.1	**13**
		C2	4.1	1.1	1.80×10^9	4.73×10^8	5.0	**7**
		C8	1.8	1.0	2.30×10^9	6.05×10^8	6.4	**14**
		C14	7.2	1.2	4.10×10^7	1.08×10^7	0.1	**15**
	$k_{overall}$ (r) (**I4** + HO˙)					**1.74×10^9**	18.6	
I14	FHT	C16	8.6	2.6	2.50×10^7	4.37×10^6	0.1	**17**
		C19	7.5	5.4	2.70×10^8	4.72×10^7	0.5	**18**
		C20	7.2	5.1	4.30×10^8	7.51×10^7	0.8	**19**
	RAF	C1	7.2	1.1	3.90×10^7	6.81×10^6	0.1	**20**
		C2	6.0	1.2	2.70×10^8	4.72×10^7	0.5	**10**
		C3	4.5	1.1	1.40×10^9	2.45×10^8	2.6	**21**
		C4	5.0	1.1	8.80×10^8	1.54×10^8	1.6	**16**
		C5	6.9	1.2	6.30×10^7	1.10×10^7	0.1	**22**
		C8	3.3	1.1	2.20×10^9	3.84×10^8	4.1	**23**
		C10	5.4	1.0	5.70×10^8	9.96×10^7	1.1	**24**
		C11	6.6	1.2	9.80×10^7	1.71×10^7	0.2	**25**
	$k_{overall}$ (r) (**I14** + HO˙)					**1.09×10^9**	11.7	
I16	FHT	C19	5.6	16.0	5.80×10^9	9.93×10^8	5.4	**26**
		C20	5.5	9.5	1.70×10^9	2.91×10^8	5.0	**27**
	RAF	C2	5.6	1.2	2.60×10^7	4.45×10^6	0.9	**1**
		C4	6.9	1.2	2.81×10^8	4.81×10^7	0.1	**28**
		C8	1.5	1.1	2.14×10^9	3.67×10^8	4.4	**29**
		C10	5.2	1.0	8.70×10^8	1.49×10^8	1.4	**30**
		C16	3.6	1.0	1.98×10^9	3.68×10^8	3.9	**31**
	$k_{overall}$ (r) (**I16** + HO˙)					**1.97×10^9**	21.0	
I17	FHT	C19	5.8	19.0	5.80×10^9	9.93×10^8	10.6	**32**
		C20	6.4	10.5	1.70×10^9	2.91×10^8	3.1	**33**
	RAF	C2	7.4	1.2	2.60×10^7	4.45×10^6	0.1	**2**
		C4	5.9	1.0	2.81×10^8	4.81×10^7	0.5	**34**
		C8	3.1	1.0	2.14×10^9	3.67×10^8	3.9	**35**
		C10	5.0	1.0	8.70×10^8	1.49×10^8	1.6	**36**
		C17	4.1	1	6.20×10^9	3.05×10^8	3.3	**37**
	$k_{overall}$ (r) (**I17** + HO˙)					**2.16×10^9**	23.0	
$k_{overall}$ (**MB** + HO˙, step 2)						**9.39×10^9**		

$k_r = r \times k_{app}$; $k_{overall}$ (r) = Σk_r; $k_{overall}$ (**MB** + HO˙, step 2) = $\Sigma k_{overall}$ (r); $\Gamma = k_r \times 100/k_{overall}$ (**MB** + HO˙, step 2); r(**I2**) = 0.202; r(**I4**) = 0.263; r(**I14**) = 0.175; r(**I16**) = 0.186; r(**I17**) = 0.171.

3.1.2. The second step reaction of diphenylamine with HO˙ in water. To better understand the interaction between intermediates and HO˙ in water, a study was undertaken on the second step of the **MB** + HO˙ reaction. The results of the calculations are presented in Tables 2, S1 (ESI)† and Fig. 3.

The results show that the intermediates exhibit high reactivity with the HO˙ radical, with an overall rate constant of the second step $k_{overall}$ (**MB** + HO˙, step 2) = 9.39×10^9 M^{-1} s^{-1}. The **I2** + ˙OH reaction has the highest rate, with $k_{overall}$ (r) (**I2** + HO˙) = 2.43×10^9 M^{-1} s^{-1} (Γ = 25.9%). This reaction is 2.2 times faster than the **I14** + ˙OH reaction ($k_{overall}$ (r) (**I14** + HO˙) = 1.09×10^9 M^{-1} s^{-1}, Γ = 11.7%). The **I4**/**16**/**17** + ˙OH reactions have moderate activity with $k_{overall}$ (r) values of 1.74×10^9 (Γ = 18.6%), 1.97×10^9 (Γ = 21.0%) and 2.16×10^9 (Γ = 23.0%), respectively. The rate constant of the second step reaction ($k_{overall}$ (**MB** + HO˙, step 2) = 9.39×10^9 M^{-1} s^{-1}) was approximately 1.1 times lower than the rate constant of the first step reaction ($k_{overall}$ (**MB** + HO˙, step 1) = 1.02×10^{10} M^{-1} s^{-1}, Table 1).

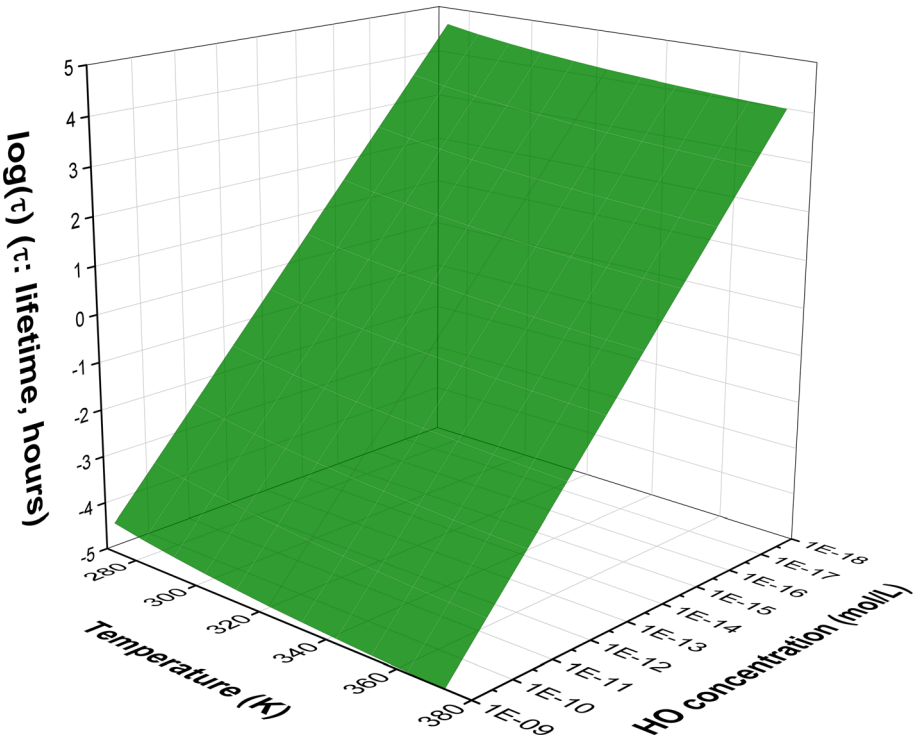

Fig. 4 Lifetime (log(τ), hours) of **MB** in water at pH > 2.0 at 273–373 K.

Fig. 3 illustrates that the two-step reaction between **MB** and ˙OH in water can potentially take place through five different pathways. The reaction can proceed initially *via* RAF(C2) followed by FHT(C20), or *via* RAF(C4/C8 or C10), resulting in the formation of cations **4** (4.3%), **7** (5.6%), **8** (5.4%) and **9** (4.3%). The RAF(C14)–RAF(C8) and RAF(C4)–RAF(C2/C14)/FHT(C20) processes produced the cations **23** (4.1%), **7** (5.0%), **14** (6.4%) and **12** (5.9%), respectively. Conversely, the FHT(C16/17)–FHT(C19/20)/RAF(C8/16/17) pathways could form the cations **26** (5.4%), **27** (5.0%), **29** (4.4%), **31** (3.9%), **32** (10.6%), **33** (3.1%), **35** (3.9%), and **37** (3.3%), respectively. Cation **32** has the largest branching ratio value, reaching 11.6%, while the other products displayed values below 7%. Overall the breakdown of **MB** by HO˙ radicals through a two-step reaction is intricate and could produce several compounds with low branching ratios (Γ < 11%).

The breakdown of **MB** by HO radicals leads to the formation of hydroxylated products (**7**, **8**, **9**, **14**, and **23**; $m/z = 316$) through the addition of two HO˙ groups to the **MB** molecule. This finding is consistent with prior experimental studies that used

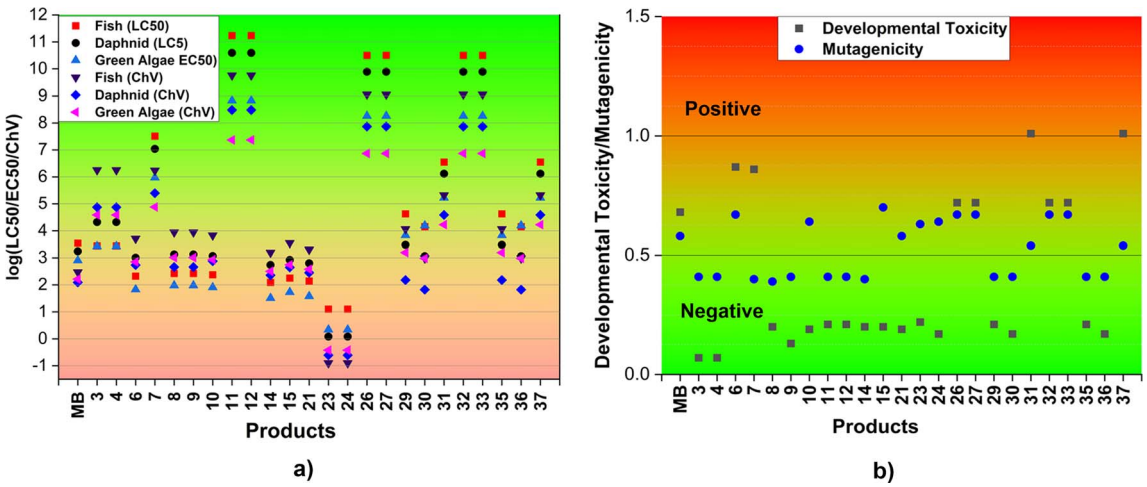

Fig. 5 Acute and chronic toxicity (log(LC_{50}/EC_{50}/ChV), mg L^{-1}) (a) and the developmental toxicity and mutagenicity (b) of **MB** and the main products (F: fish; D: daphnia; GA: green algae).

ESI-MS to analyze the breakdown of **MB** by HO˙ radicals.[10,11,28] Our calculations also highlighted that the addition reaction can only occur in even positions (C2, C4, C8, C10, or C14), but not in odd positions such as the C1 and C11 positions (Fig. 1) as shown in previous studies.[10,11,28] Hence, the computational approach uncovered details of the **MB** breakdown process that experimental observations failed to reveal.

3.2. Environmental risk assessment

3.2.1. Environmental lifetimes. The attribute of environmental persistence of a compound is highly significant for its environmental safety as a lack of breakdown processes means a compound retains its toxicity allowing its transportation to distant regions.[72] In the presence of HO˙ radicals in water at a temperature range of 273–373 K, with environmentally relevant pH values (pH > 2.0, **MB** > 99%), and with $[HO^{\bullet}] = 10^{-18}$ to 10^{-15} M in natural water[25–27] and 10^{-10} to 10^{-9} M in AOP-treated wastewater,[76] the lifetime of **MB** was calculated (Fig. 4 and Table S2, ESI†). In water, **MB** degrades within 5.17×10^{-5} to 5.04×10^{4} hours in the range of $[HO^{\bullet}] = 10^{-18}$ to 10^{-9} M (Table S2, ESI†). Specifically, the degradation of **MB** in the AOP-treated wastewater can occur within a second (0.04–1.82 s), whereas in natural water, it can occur in 11.66 to 5.04×10^{4} hours ($\log(\tau) =$ 1.07–4.70) (*i.e.* 11.66 hours to 5.76 years) in the 273–373 K temperature range. For a given $[HO^{\bullet}]$ concentration, the value of τ decreases as the temperature increases. Thus, the lifetime of ˙OH-degraded **MB** in natural water environments is estimated to be between 50.4 and 5.04×10^{4} hours ($\log(\tau) = 1.70$–4.70) at a low temperature, which decreases to 11.66–1.17×10^{4} hours ($\log(\tau) = 1.07$–4.07) at 373 K.

3.2.2. Ecological toxicity, developmental toxicity and mutagenicity. To evaluate the environmental effects of **MB** and its breakdown products, we analyze the acute and chronic toxicity towards three aquatic organisms: fish, daphnia, and green algae. The estimation is based on the reaction outcomes and the ECOSAR program. Fig. 5a and Table S3, ESI† depict the results. Previous research has shown that substances with LC_{50}/EC_{50}/ChV (mg L^{-1}) values lower than 100 ($\log(LC_{50}/EC_{50}/ChV) \leq 2$) are harmful to green algae, fish, and daphnia.[67,77] The log values for LC_{50}/EC_{50}/ChV of all the species examined for products **23** and **24** are less than 2. This result indicates that the chemicals demonstrate toxicity against three distinct groups of aquatic organisms. The products **3**, **4**, **7**, **11**, **12**, **26**, **27**, **29**, **31**, **32**, **33**, **35**, and **37**, as well as **MB**, might not cause damage to fish, daphnia, or green algae. The degradation products **6**, **8**, **9**, **10**, **14**, **15** and **21** may be harmful with green algae (EC_{50}(green algae) < 2), whereas the products **30** and **36** will be hazardous with daphnid (ChV(daphnid) < 2). Therefore, it is crucial to consider the possible ecological consequences linked to the degradation process of **MB**.

In order to assess the impact of **MB** and its breakdown products on living creatures, the developmental toxicity and mutagenicity of these compounds were also determined using T.E.S.T. The corresponding outcomes are illustrated in Fig. 5b and Table S3, ESI.† The results imply that products **6**, **7**, **26**, **27**, **31**, **32**, **33**, and **37**, along with **MB** may have developmental toxicity, as indicated by toxicity values for development that are higher than 0.5. These substances have the ability to disrupt the processes of nucleic acid translation and expression, potentially affecting the growth and development of humans.[71] Simultaneously, the calculations indicate that the products **6**, **10**, **15**, **21**, **23**, **24**, **26**, **27**, **31**, **32**, **33**, and **37**, as well as **MB**, may present mutagenic hazards (mutagenicity values ≥ 0.5). The rest of the products, specifically **3**, **4**, **8**, **9**, **11**, **12**, **14**, **29**, **30**, **35**, and **36**, do not exhibit any developmental toxicity or mutagenicity. This can be explained by the structural change where the addition reaction has the potential to disrupt the aromatic ring of **MB** which is mostly responsible for its toxicity.

3.2.3. Bioconcentration, biodegradability. The level of harm caused to organisms is directly related to the amount of exposure they have to reactants and the substances produced when those reactants break down. Estimating bioaccumulation serves as a rational method for measuring the degree of exposure to a chemical.[78] **MB** builds up in organisms through various processes, leading to negative health impacts and an increase in ecological toxicity. Bioconcentration factors (BCFs) of **MB** and its transformation products can be estimated using the BCFBAF module of EPISUITE. Typically, the accumulation of substances in fish tissues increases as the bioconcentration factor (BCF) of the organic matter increases. This is seen in Table S3, ESI.† A chemical is deemed to possess substantial bioaccumulation potential if its bioconcentration factor (BCF) exceeds 5000.[79] The results indicate that the interaction between the degradation products of **MB** and the HO˙ radical in a two-step reaction does not have an effect on the BCF values. Consequently, the BCF values of the products closely resembled that of the initial material (3.162). Hence, the likelihood of organisms accumulating **MB** and its breakdown products may not be substantial.

The biodegradability of the reactant **MB** and its degradation products was assessed using the BIOWIN 3, 4, and 5 models incorporated in the EPISUITE program (Table S3, ESI†).[72] The results obtained from the BIOWIN models suggest that degradation products undergo initial biodegradation during a period ranging from a few days to months, while both the **MB** and degradation products may not be biodegradable. Consequently, the breakdown of **MB** by HO˙ radicals in the two-step process could result in the formation of non-biodegradable substances. However, these substances may not accumulate in living organisms.

4. Conclusion

A computational analysis was conducted to study the breakdown pathways of **MB** in the presence of HO˙. An assessment of the thermodynamic and kinetic parameters of possible reaction paths was conducted in order to ascertain the most probable products. It was found that in natural water bodies **MB** can undergo degradation with lifetimes in the broad range of 11.66 to 5.04×10^{4} hours (*i.e.* 11.66 hours to 5.76 years). The HO˙ + **MB** reaction in water can take place *via* either FHT or RAF mechanism. The addition reaction is possible at carbon atoms at most even positions C2, C4, C8, C10, or C14, but not at odd

positions. The intermediates and some of the products generated in the process can pose a threat to aquatic organisms, including fish, daphnia, and green algae. Additionally, they have the potential to induce developmental toxicity and have poor biodegradability. However, the introduction of the HO radical to the aromatic ring might lead to the creation of compounds that do not exhibit any developmental toxicity or mutagenicity. Hence, **MB** poses a moderate environmental risk with a mix of safe and toxic breakdown products.

Data availability

The data supporting this article have been included as part of the ESI.†

Conflicts of interest

There are no conflicts to declare.

Acknowledgements

This research is funded by the Vietnamese Ministry of Education and Training under project number B2024.DNA.09.

References

1 M. I. Din, R. Khalid, J. Najeeb and Z. Hussain, *J. Cleaner Prod.*, 2021, **298**, 126567.
2 M. Rafatullah, O. Sulaiman, R. Hashim and A. Ahmad, *J. Hazard. Mater.*, 2010, **177**, 70–80.
3 M. Mohammed, A. Shitu and A. Ibrahim, *Res. J. Chem. Sci.*, 2014, **4**, 91–102.
4 W. Subramonian and T. Y. Wu, *Water, Air, Soil Pollut.*, 2014, **225**, 1–15.
5 T. Liu, Y. Li, Q. Du, J. Sun, Y. Jiao, G. Yang, Z. Wang, Y. Xia, W. Zhang and K. Wang, *Colloids Surf., B*, 2012, **90**, 197–203.
6 A. Sipos and H. Urakawa, *Lett. Appl. Microbiol.*, 2016, **62**, 199–206.
7 M. Wainwright and K. Crossley, *J. Chemother.*, 2002, **14**, 431–443.
8 M. Oz, D. E. Lorke and G. A. Petroianu, *Biochem. Pharmacol.*, 2009, **78**, 927–932.
9 C.-H. Wu and J.-M. Chern, *Ind. Eng. Chem. Res.*, 2006, **45**, 6450–6457.
10 C. Luo, S. Wang, D. Wu, X. Cheng and H. Ren, *Environ. Technol. Innovation*, 2022, **25**, 102198.
11 R. K. Singh, V. Babu, L. Philip and S. Ramanujam, *J. Water Process Eng.*, 2016, **11**, 118–129.
12 H. Valdés, R. F. Tardón and C. A. Zaror, *Chem. Eng. J.*, 2012, **211**, 388–395.
13 A. Syoufian and K. Nakashima, *J. Colloid Interface Sci.*, 2008, **317**, 507–512.
14 C. Minamoto, N. Fujiwara, Y. Shigekawa, K. Tada, J. Yano, T. Yokoyama, Y. Minamoto and S. Nakayama, *Chemosphere*, 2021, **263**, 128141.
15 D. Wen, W. Li, J. Lv, Z. Qiang and M. Li, *J. Hazard. Mater.*, 2020, **391**, 121855.
16 N. T. Hoang, T. D. Manh, V. T. Nguyen, N. T. T. Nga, F. M. Mwazighe, B. D. Nhi, H. Y. Hoang, S. W. Chang, W. J. Chung and D. D. Nguyen, *Chemosphere*, 2022, **308**, 136457.
17 Z. Eren and K. O'Shea, *J. Environ. Eng.*, 2019, **145**, 04019070.
18 F. Banat, S. Al-Asheh and M. Nusair, *Desalination*, 2005, **181**, 225–232.
19 Z. Wang, H. Zhao, H. Qi, X. Liu and Y. Liu, *Environ. Technol.*, 2019, **40**, 1138–1145.
20 A. Houas, H. Lachheb, M. Ksibi, E. Elaloui, C. Guillard and J.-M. Herrmann, *Appl. Catal., B*, 2001, **31**, 145–157.
21 A. Mills, *Appl. Catal., B*, 2012, **128**, 144–149.
22 R. H. Waghchaure, V. A. Adole and B. S. Jagdale, *Inorg. Chem. Commun.*, 2022, **143**, 109764.
23 P. P. Vaughan and N. V. Blough, *Environ. Sci. Technol.*, 1998, **32**, 2947–2953.
24 K. Takeda, H. Takedoi, S. Yamaji, K. Ohta and H. Sakugawa, *Anal. Sci.*, 2004, **20**, 153–158.
25 H. Xu, Y. Li, J. Liu, H. Du, Y. Du, Y. Su and H. Jiang, *Water Res.*, 2020, **176**, 115774.
26 S. A. Timko, C. Romera-Castillo, R. Jaffé and W. J. Cooper, *Environ. Sci.: Processes Impacts*, 2014, **16**, 866–878.
27 D. Vione, G. Falletti, V. Maurino, C. Minero, E. Pelizzetti, M. Malandrino, R. Ajassa, R.-I. Olariu and C. Arsene, *Environ. Sci. Technol.*, 2006, **40**, 3775–3781.
28 K. Sharma, R. K. Vyas and A. K. Dalai, *J. Chem. Eng. Data*, 2017, **62**, 3651–3662.
29 D. Kobayashi, C. Honma, H. Matsumoto, T. Takahashi, C. Kuroda, K. Otake and A. Shono, *Ultrason. Sonochem.*, 2014, **21**, 1489–1495.
30 I. A. Salem and M. S. El-Maazawi, *Chemosphere*, 2000, **41**, 1173–1180.
31 A. Galano and J. R. Alvarez-Idaboy, *J. Comput. Chem.*, 2013, **34**, 2430–2445.
32 M. E. Alberto, N. Russo, A. Grand and A. Galano, *Phys. Chem. Chem. Phys.*, 2013, **15**, 4642–4650.
33 N. T. Hoa and Q. V. Vo, *Chemosphere*, 2023, **314**, 137682.
34 P. A. Denis and F. R. Ornellas, *J. Phys. Chem. A*, 2009, **113**, 499–506.
35 P. A. Denis, *J. Phys. Chem. A*, 2006, **110**, 5887–5892.
36 A. Galano, G. Mazzone, R. Alvarez-Diduk, T. Marino, J. R. Alvarez-Idaboy and N. Russo, *Annu. Rev. Food Sci. Technol.*, 2016, **7**, 335–352.
37 A. Galano and J. R. Alvarez-Idaboy, *J. Comput. Chem.*, 2014, **35**, 2019–2026.
38 M. G. Evans and M. Polanyi, *Trans. Faraday Soc.*, 1935, **31**, 875–894.
39 H. Eyring, *J. Chem. Phys.*, 1935, **3**, 107–115.
40 D. G. Truhlar, W. L. Hase and J. T. Hynes, *J. Phys. Chem.*, 1983, **87**, 2664–2682.
41 T. Furuncuoglu, I. Ugur, I. Degirmenci and V. Aviyente, *Macromolecules*, 2010, **43**, 1823–1835.
42 E. Vélez, J. Quijano, R. Notario, E. Pabón, J. Murillo, J. Leal, E. Zapata and G. Alarcón, *J. Phys. Org. Chem.*, 2009, **22**, 971–977.
43 E. Dzib, J. L. Cabellos, F. Ortíz-Chi, S. Pan, A. Galano and G. Merino, *Int. J. Quantum Chem.*, 2019, **119**, e25686.

44 E. Dzib, J. L. Cabellos, F. Ortiz-Chi, S. Pan, A. Galano and G. Merino, *Eyringpy 1.0.2*, Cinvestav, Mérida, Yucatán, 2018.
45 E. Pollak and P. Pechukas, *J. Am. Chem. Soc.*, 1978, **100**, 2984–2991.
46 A. Fernández-Ramos, B. A. Ellingson, R. Meana-Pañeda, J. M. Marques and D. G. Truhlar, *Theor. Chem. Acc.*, 2007, **118**, 813–826.
47 C. Eckart, *Phys. Rev.*, 1930, **35**, 1303.
48 R. A. Marcus, *Annu. Rev. Phys. Chem.*, 1964, **15**, 155–196.
49 R. A. Marcus, *Rev. Mod. Phys.*, 1993, **65**, 599.
50 S. F. Nelsen, S. C. Blackstock and Y. Kim, *J. Am. Chem. Soc.*, 1987, **109**, 677–682.
51 S. F. Nelsen, M. N. Weaver, Y. Luo, J. R. Pladziewicz, L. K. Ausman, T. L. Jentzsch and J. J. O'Konek, *J. Phys. Chem. A*, 2006, **110**, 11665–11676.
52 F. C. Collins and G. E. Kimball, *J. Colloid Sci.*, 1949, **4**, 425–437.
53 M. Von Smoluchowski, *Z. Phys. Chem.*, 1917, **92**, 129–168.
54 D. G. Truhlar, *J. Chem. Educ.*, 1985, **62**, 104.
55 A. Einstein, *Ann. Phys.*, 1905, **17**, 549–560.
56 G. G. Stokes, *Mathematical and Physical Papers*, University Press, Cambridge, 1905.
57 S. Benson, *The Foundations of Chemical Kinetics*, Malabar, Florida, 1982.
58 J. R. Alvarez-Idaboy, L. Reyes and N. Mora-Diez, *Org. Biomol. Chem.*, 2007, **5**, 3682–3689.
59 J. R. Alvarez-Idaboy, N. Mora-Diez, R. J. Boyd and A. Vivier-Bunge, *J. Am. Chem. Soc.*, 2001, **123**, 2018–2024.
60 M. Carreon-Gonzalez, A. Vivier-Bunge and J. R. Alvarez-Idaboy, *J. Comput. Chem.*, 2019, **40**, 2103–2110.
61 N. Mora-Diez, J. R. Alvarez-Idaboy and R. J. Boyd, *J. Phys. Chem. A*, 2001, **105**, 9034–9039.
62 J. R. l. Alvarez-Idaboy and A. Galano, *J. Phys. Chem. B*, 2012, **116**, 9316–9325.
63 Y. Zhao and D. G. Truhlar, *Theor. Chem. Acc.*, 2008, **120**, 215–241.
64 A. V. Marenich, C. J. Cramer and D. G. Truhlar, *J. Phys. Chem. B*, 2009, **113**, 6378–6396.
65 Q. V. Vo, M. V. Bay, P. C. Nam, D. T. Quang, M. Flavel, N. T. Hoa and A. Mechler, *J. Org. Chem.*, 2020, **85**, 15514–15520.
66 Q. V. Vo, N. T. Hoa and A. Mechler, *Polym. Degrad. Stab.*, 2021, **185**, 109483.
67 Q. Mei, J. Sun, D. Han, B. Wei, Z. An, X. Wang, J. Xie, J. Zhan and M. He, *Chem. Eng. J.*, 2019, **373**, 668–676.
68 J. Sun, B. Wei, Q. Mei, Z. An, X. Wang and M. He, *Chem. Eng. J.*, 2019, **358**, 456–466.
69 S. Luo, Z. Wei, D. D. Dionysiou, R. Spinney, W.-P. Hu, L. Chai, Z. Yang, T. Ye and R. Xiao, *Chem. Eng. J.*, 2017, **327**, 1056–1065.
70 Y. Gao, Y. Ji, G. Li and T. An, *Water Res.*, 2016, **91**, 77–85.
71 *Toxicity Estimation Software Tool; A Program to Estimate Toxicity from Molecular Structure*, U.S. EPA, 2020.
72 R. S. Boethling, D. G. Lynch, J. S. Jaworska, J. L. Tunkel, G. C. Thom and S. Webb, *Environ. Toxicol. Chem.*, 2004, **23**, 911–920.
73 Q. V. Vo, N. T. Hoa and A. Mechler, *New J. Chem.*, 2021, **45**, 17683–17691.
74 O. Impert, A. Katafias, P. Kita, A. Mills, A. Pietkiewicz-Graczyk and G. Wrzeszcz, *Dalton Trans.*, 2003, 348–353.
75 B. N. Ames, M. K. Shigenaga and T. M. Hagen, *Proc. Natl. Acad. Sci. U.S.A.*, 1993, **90**, 7915–7922.
76 J. M. Burns, W. J. Cooper, J. L. Ferry, D. W. King, B. P. DiMento, K. McNeill, C. J. Miller, W. L. Miller, B. M. Peake and S. A. Rusak, *Aquat. Sci.*, 2012, **74**, 683–734.
77 P. Reuschenbach, M. Silvani, M. Dammann, D. Warnecke and T. Knacker, *Chemosphere*, 2008, **71**, 1986–1995.
78 N. Wang, L. He, X. Sun, X. Li and M. Li, *J. Hazard. Mater.*, 2022, **427**, 127941.
79 M.-J. He, X.-J. Luo, M.-Y. Chen, Y.-X. Sun, S.-J. Chen and B.-X. Mai, *Sci. Total Environ.*, 2012, **419**, 109–115.